

# Product Recirculation and Mixing Studies in a Stagnation Point Reverse Flow Combustor

Mohan K. Bobba,\* Priya Gopalakrishnan,\* Karthik Periagaram,\* Jerry M. Seitzman†

*School of Aerospace Engineering  
Georgia Institute of Technology  
Atlanta, GA, USA*

Gas turbine combustor design is being driven towards leaner operation to conform to increasingly stringent emissions regulations. The low temperatures reduce NOx emissions but adversely impact the stability of the combustor. A novel combustor design, referred to as a Stagnation-Point Reverse-Flow (SPRF) combustor, was recently developed that is able to operate stably at very lean fuel-air mixtures, over a range of loadings, and with low NOx emissions making it an exciting option for ground power and aircraft gas turbines. Various optical diagnostic techniques are employed to investigate the flame and mixing characteristics of the SPRF combustor operating at atmospheric pressure. These measurements include chemiluminescence imaging, Particle Image Velocimetry (PIV) for velocity fields and Spontaneous Raman Scattering (SRS) for species concentrations. This unique reverse flow design allows hot product gases to mix with and preheat the incoming reactants. The flow reversal also gives rise to a low velocity stagnation zone in the combustor with a high turbulence level facilitating robust flame stabilization over a variety of flow conditions. Product entrainment has been quantified in terms of the recirculation ratio ( $K_v$ ), defined as the ratio of recirculated mass of product gas to the mass of fuel and air entering the flame zone. Although reactants are found to burn in a highly preheated (1300 K) and turbulent environment due to mixing with hot product gases, the residence times are sufficiently long compared to the ignition timescales such that the reactants do not autoignite. Turbulent flame structure analysis indicates that the flame is primarily in the thin reaction zones regime throughout the combustor. The flame tends to become more flamelet like, however, for increasing distance from the injector. Fuel-air mixing measurements indicate that the fuel is shielded from hot products until it is fully mixed with air, providing almost premixed performance without its associated safety issues. The effect of changing the air injector dimensions on the mixing of fuel and air is also investigated.

## I. Introduction

The drive towards reduced pollutant emissions has prompted the gas turbine industry to develop cleaner, more environmentally friendly power and propulsion systems, while simultaneously maintaining (or improving) efficiency, operability and performance. The production of NOx tends to be a strong function of temperature, so the residence time in regions of high temperature is of particular importance. The methods to reduce NOx emissions are, therefore, typically based on schemes to reduce peak flame temperature or the residence time in regions of high temperature.<sup>1,2</sup> Lean premixed combustion systems have been used to lower the flame temperatures and for avoiding stoichiometry non-uniformities that arise due to incomplete mixing of fuel and air. One of the major challenges facing designers of such combustion systems is the flame stability at these lean conditions as the weaker combustion process is more vulnerable to small perturbations in combustor operating conditions. Flame stability in such systems can be enhanced in various ways, including reactant preheating and exhaust gas recirculation. Gupta<sup>3,4</sup> reported that

---

\* Graduate Research Assistant (AIAA Student Member)

† Associate Professor (AIAA Associate Fellow)

flames with highly preheated combustion air were much more stable and homogeneous (both temporally and spatially) as compared to room-temperature combustion air and hence could operate at much leaner equivalence ratios. However, the reduction in NO<sub>x</sub> emission levels due to leaner operation is partially offset by the increased flame temperature due to preheating.

Another difficulty in the operation of premixed systems is flame flashback and autoignition. High temperatures in a premixer can thus result in damage or shutdown of an engine. Hence, it is advantageous if fuel and air can be injected into the combustor separately. Fuel-air mixing mechanisms are determined and controlled by design of the geometry and aerodynamics of the burner and enclosure, which also influence residence times. The use of high velocity coaxial air in jet diffusion flames<sup>5</sup> has been successfully demonstrated to reduce NO<sub>x</sub> emission levels in hydrocarbon flames. Increased shear produced by the high velocity coaxial air results in enhanced mixing between fuel and air before combustion and also lowers the residence times resulting in lower emission levels. Towards this end, an attractive scheme is staged combustion, with staging performed on either the fuel<sup>6</sup> or air<sup>7</sup> introduction. This requires, however, sophisticated designs with increased capital investment.

In a recent paper, Kalb *et al.*<sup>8</sup> suggested that NO<sub>x</sub> emissions could be reduced to ultra low levels by mixing a reactant mixture with hot combustion products laden with radicals prior to combustion. They argued that the presence of radicals in the mixture lowers its ignition temperature and, thus, allows stable combustion of mixtures that would otherwise not be flammable. Thus, premixing the reactants with radicals to lower the combustion process temperature should allow low temperature combustion with ultra low NO<sub>x</sub> emissions.

In combustors with extensive exhaust gas recirculation, the amount of product entrainment is typically quantified by a single quantity such as the exhaust recirculation ratio ( $K_v$ ), which is normally defined to be the ratio of mass flow rate of products to that of the reactants previous to reactant combustion;

$$K_v = \frac{\dot{m}_E}{\dot{m}_F + \dot{m}_A}$$

where the subscripts, E, F and A stand for recirculated exhaust gas, the fuel and combustion air respectively.

Wunning *et al.*<sup>1</sup> have identified flame stability limits for furnace combustors over a range of recirculation ratios and process temperatures. It was suggested that stable flames are possible over a whole range of combustor chamber temperature if the air is not significantly vitiated ( $K_v < 0.3$ ). For moderately high recirculation rates ( $0.3 < K_v < 2.5$ ), they found the flame becomes unstable and is found to lift-off and finally blowout. If the diluted air temperature is over the fuel autoignition temperature and the recirculation ratio ( $K_v$ ) exceeds 2.5, the fuel can react in a very stable form of combustion known as ‘flameless oxidation’. Although operation in this mode provides reduction in NO<sub>x</sub> emissions by facilitating combustion at an ultra lean stoichiometry, the reduced burning intensity demands large combustion chambers that are undesirable in applications where space and weight come at a premium.

To meet these stringent requirements, a simple and compact combustor design called the Stagnation-Point Reverse-Flow (SPRF) combustor incorporating some of the above mentioned methodologies has recently been demonstrated.<sup>9</sup> The combustor design consists of a tube that is open at one end and closed at the other. As seen in the flow schematic of the combustor in Figure 1, the reactants are injected along the combustor center line without any swirl, while the products flow in the reverse direction to exit the combustor. Products leaving the combustor flow over the injector, providing “internal” preheating of the reactants before injection.

This configuration is found to operate *stably* with ultra low NO<sub>x</sub> emissions in both premixed and non-premixed modes of operation over a wide range of combustor operating conditions. Figure 2a shows the NO<sub>x</sub> emissions at the exit of the premixed SPRF combustor for various equivalence ratios plotted as a function of the adiabatic flame temperature. The NO<sub>x</sub> emissions measured in this combustor are found to be below 1 ppm for the leanest operating condition ( $\phi \sim 0.51$ ). For comparison, the figure also shows NO<sub>x</sub> levels from a laminar, one-dimensional, premixed flame, based on a CHEMKIN simulation and the GRIMech 3.0 mechanism<sup>10</sup> over a range of equivalence ratios. The model results represent the NO<sub>x</sub> produced in the flame front, i.e., where the heat release has dropped to 1% of its peak value, as opposed to thermal NO<sub>x</sub> produced in the product gases. In this sense, the model results represent a

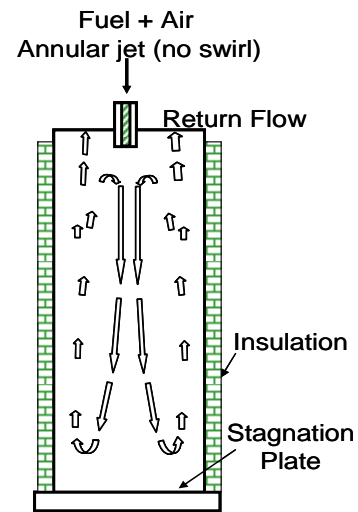


Figure 1. Schematic of the SPRF combustor.

minimum expected emission level for a premixed flame at a given stoichiometry. The measured emissions from the combustor are reasonably close to the minimum levels, until the flame temperatures exceed  $\sim 1800\text{-}1900\text{ K}$ , where thermal  $\text{NO}_x$  formation in the post-flame region is expected to become dominant. While the  $\text{NO}_x$  emissions are comparable to other premixed combustors, the SPRF combustor is able to produce a compact, stable flame even under very lean conditions, without external preheating or swirl. For example, the leftmost point in Figure 2a was acquired with the combustor operating at  $\phi=0.51$  and with a combustor power density of  $20\text{ MW/m}^3$  (at atmospheric pressure).

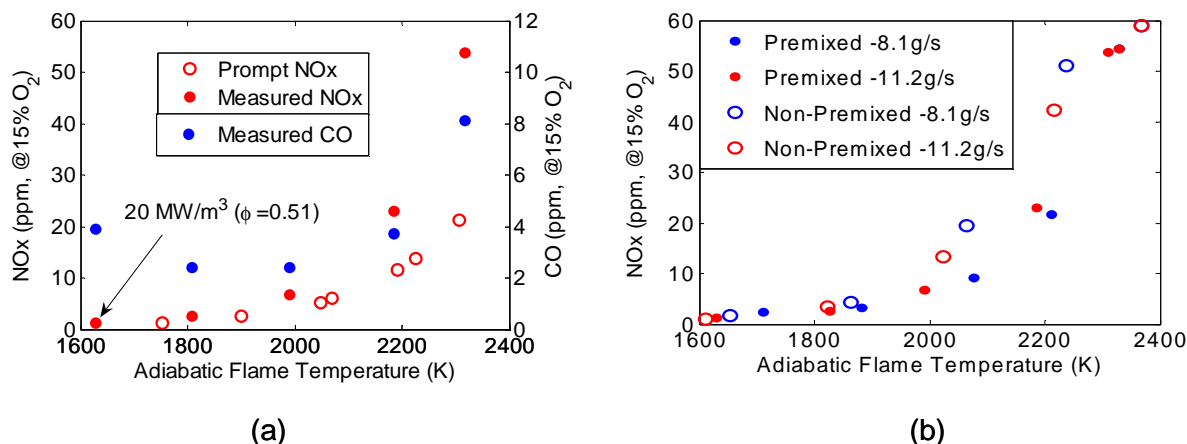


Figure 2. Variation of  $\text{NO}_x$  emissions with adiabatic flame temperature based on overall equivalence ratio and measured inlet temperature in (a) premixed case in comparison to a laminar flame model and (b) in non-premixed mode in comparison to the premixed case.

One of the key features of the SPRF combustor is its inherent flexibility to operate in both premixed and non-premixed modes. The emissions levels obtained in non-premixed mode were found to be very close to those obtained in the premixed mode of operation, as shown in Figure 2b. Again, it is seen that loading does not have a significant effect on the emission levels. Since premixing requires added hardware and introduces the possibility of flashback or autoignition in the premixer, non-premixed operation is definitely advantageous.

Thus, this current work will examine the features of the combustor that contribute to its stability and low  $\text{NO}_x$  emissions even with non-premixed fuel injection. The requirements for good emission performance and producing a stable flame for both non-premixed and premixed flames are closely associated with local flow and burning velocities, and mixture preparation. So it is necessary to understand the mixing characteristics in the SPRF combustor. Various non-intrusive optical diagnostic techniques are employed. Imaging of chemiluminescence from  $\text{CH}^*$  and  $\text{CO}_2^*$  serves as an indicator of heat release rate in premixed hydrocarbon flames. Flow field information is obtained with the use of Particle image Velocimetry (PIV). These techniques have been successfully used to study similar confined turbulent jet flame configurations.<sup>11</sup> Lastly, Spontaneous Raman Scattering (SRS)<sup>12</sup> is employed to quantify mixing of fuel with air and hot products through instantaneous point measurements of the mole fractions of all major species. This is one of the few quantitative techniques that provide spatially and temporally resolved simultaneous multi-species concentrations of major combustion products ( $\text{N}_2$ ,  $\text{O}_2$ ,  $\text{CO}_2$ ,  $\text{H}_2\text{O}$  and  $\text{CH}_4$ ) and an estimate of the local temperature.

## II. Experimental Setup

The SPRF combustor operating at atmospheric pressure, used here consists of a central injector located at the open end of a 70 mm diameter ( $D_c$ ) and 304.8 mm long (L) quartz tube as seen in Figure 3a. The 12.5 mm diameter (D) injector is formed by two concentric tubes, with premixed natural gas and air flowing through the annulus. For non-premixed operation, the central tube is used for fuel injection as shown in Figure 3a. Fuel and air flow rates are monitored with calibrated rotameters, and the two flows are mixed well upstream of the injector. A quartz base plate forms the closed end of the tube and allows introduction of a laser sheet for PIV and Raman measurements. The combustor is also insulated with a hollow alumina cylinder with an inner diameter that is slightly larger than the outer diameter of the quartz tube. The insulation is cut into four segments; one of these has a  $\sim 150^\circ$  section removed to form a window for optical access. Thus only one-quarter of the length of the combustor can be imaged with the insulation installed; the complete combustor is mapped by moving the window segment to a different axial location.

Because the product gases exiting the combustor flow over the injector, the temperature of the incoming reactants increases. To monitor this internal preheating, an unshielded thermocouple (K type) can be placed in the injector annulus, roughly 4 mm upstream of the injector exit plane. The thermocouple is not present during the optical diagnostic measurements.

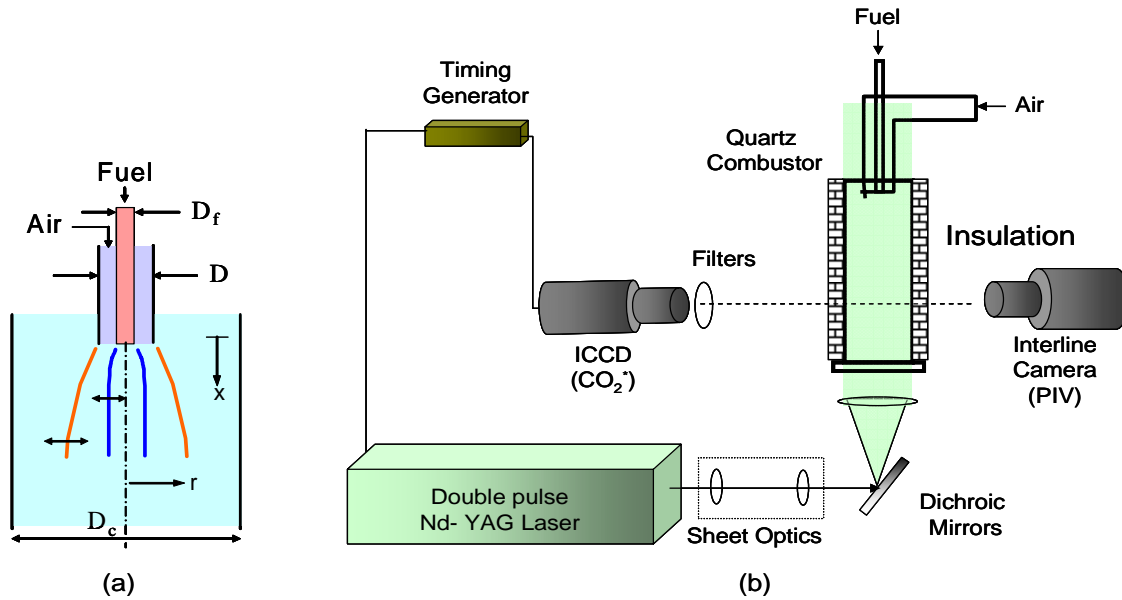


Figure 3. (a) SPRF combustor injector configuration and (b) layout of PIV and chemiluminescence imaging setup.

For velocity measurements using PIV, the combustion air is seeded with 1-2  $\mu\text{m}$  aluminum oxide particles before being mixed with the fuel. The two PIV laser pulses are provided by the second harmonic outputs of a dual-head, Nd:YAG laser (Continuum Surelite I-10) as shown in Figure 3b. The delay between the pulse pairs is varied with an external pulse generator. The output beams are converted into a sheet (68 $\times$ 0.6 mm) with three cylindrical lenses. The particle scattering images produced by a pair of laser pulses are recorded with a 12-bit interline CCD camera (MicroMAX, 1300 $\times$ 1030) equipped with a 50 mm Nikkor (f/1.8) lens and synchronized to the lasers. For the current measurements, the pulse energies for the each laser were  $\sim 90$  mJ, and the pulse delay varied from 3 to 11  $\mu\text{s}$ . A FFT based cross-correlation technique is employed to find the average particle displacement and hence the local velocity. Each vector represents the average velocity in an interrogation volume 2.19 $\times$ 2.19 $\times$ 0.4  $\text{mm}^3$ .

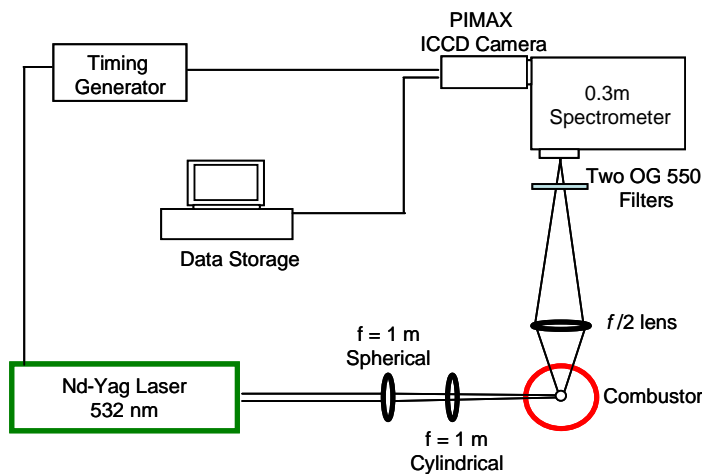


Figure 4. Optical layout of Spontaneous Raman Scattering (SRS) setup.

The natural chemiluminescence from the combustor is also collected at right angles to the sheet with a second intensified camera (Princeton Instruments ICCD-576-S/RB-E, 18 mm intensifier, 384 $\times$ 576) equipped with a narrow-band interference filter (430 $\pm$ 5 nm), which passes  $\text{CH}^*$  and a small portion of the broadband  $\text{CO}_2^*$  chemiluminescence. The camera is set to view to full width of the combustor which results in a pixel resolution of  $\sim 250$   $\mu\text{m}$  with an exposure time of 250  $\mu\text{s}$ .

Mole fractions of major species are measured using Raman scattering using the second harmonic (532 nm) of an Nd:YAG laser (Quanta-Ray Pro-250, Spectra Physics) operating in a Q-switched mode was used. It was triggered at 10 Hz to produce pulses of 250 mJ per pulse. The pulse energy was limited in order to prevent the breakdown of the gases in the measurement volume and to avoid

damaging the quartz glass of the SPRF combustor. The laser beam was focused to illuminate a measurement volume of  $2 \times 2 \times 0.3 \text{ mm}^3$  by passing it through a 1 m focal length convex lens (50.8 mm diameter) followed by a 1 m focal length cylindrical lens (25.4 mm  $\times$  50.8 mm) as seen in Figure 4. The Raman scattering signal is collected at a  $90^\circ$  angle relative to the beam propagation direction using a 160 mm focal length spherical lens (80 mm diameter). The collected light is focused onto the 300  $\mu\text{m}$  slit of a 0.3 m spectrometer ( $f/4$ , SpectraPro-300i, Acton Research Corporation) at  $f/5.3$  and a magnification of 0.5. A combination of two OG 550 Schott glass filters is used to attenuate the Rayleigh and Mie scattered light (from dust particles) entering the spectrometer. The incident light is dispersed by the spectrometer using a 300 grooves/mm grating, and is then recorded on a PI Acton ICCD camera (512 $\times$ 512 pixels). The spectral range from 555 to 685 nm is captured with a resolution of 0.256 nm/pixel. The camera is equipped with an 18 mm (Gen III, HB filmless) intensifier tube with 30% quantum efficiency in the visible range. The intensifier is gated on for 50 ns window synchronized with the laser pulse. This short gate timing helps reject background emissions from the flame and blackbody radiation from the combustor walls. The collected spectra were binned on chip over 170 pixels in the spatial direction to increase the signal-to-noise ratio of the measurements, resulting in a spatial resolution of 2 mm along the laser beam. The combustor and injector assembly are mounted on a traversing platform, while the optics setup remains fixed. This configuration allowed us to make instantaneous single point Raman measurements from the injector plane to 200 mm into the combustor along the centerline axially or to 30 mm from the centerline radially.

Raman signals are obtained from the background subtracted spectra by integrating under the respective peaks for each species. Figure 5 shows a typical single shot spectrum recorded close to the injector in SPRF combustor operating on premixed  $\text{CH}_4$  and air. The Raman signal ( $S_i$ ) is proportional to the number density of the scattering species and can be expressed in terms of species mole fractions ( $X_i$ ) and temperature ( $T$ ), i.e.,

$$S_i = \frac{C_i X_i}{T}$$

Assuming  $\text{CO}_2$ ,  $\text{O}_2$ ,  $\text{N}_2$ ,  $\text{CH}_4$ ,  $\text{H}_2\text{O}$  are the only major species present, then including the additional constraint

$$\sum X_i = 1$$

provides a complete set of equations. The calibration constants  $C_i$  for  $\text{CO}_2$ ,  $\text{O}_2$ ,  $\text{N}_2$ , and  $\text{CH}_4$  are determined from measurements obtained at the exit of a preheated (300–800 K) laminar jet with a known concentration gas mixture. The calibration constants are found to vary less than 5% across the reactant temperature range of interest. The Raman signal for  $\text{H}_2\text{O}$  is calibrated with measurements at the exit of the SPRF combustor (at  $\phi=0.58$ ), where the equilibrium water concentration is known to be essentially twice the  $\text{CO}_2$  concentration. A matrix formulation<sup>12</sup> is used to solve the above complete set of equations to find mole fractions of  $\text{CO}_2$ ,  $\text{O}_2$ ,  $\text{N}_2$ ,  $\text{CH}_4$ ,  $\text{H}_2\text{O}$  and local temperature.

Signal interpretation can be complicated by fluorescence interferences from PAH and soot or due to overlap of Raman rotation and vibration bands from different species.<sup>12</sup> The fluorescence interferences are expected to be negligible in the current work due to lean operation of the methane-fueled combustor. Overlap in Raman spectra is most prominent between  $\text{CO}_2$ ,  $\text{O}_2$  and  $\text{CH}_4$ . These interferences are corrected based on calibration spectra obtained at 300 K as outlined by Miles.<sup>13</sup>

### III. Results and Discussion

The requirements for good emission performance and producing a stable flame for both non-premixed and premixed flames are closely associated with local flow and burning velocities, and mixture preparation. So it is necessary to understand the flame and mixing characteristics in the SPRF combustor. We begin by studying the velocity field in the combustor. As previously reported,<sup>14</sup> the time-averaged flowfield in this unique reverse flow configuration is shown in Figure 6a as a combination of axial velocity contours and interpolated streamlines. This velocity field corresponds to the premixed SPRF combustor with a 12.5 mm injector (D) operating with a total mass

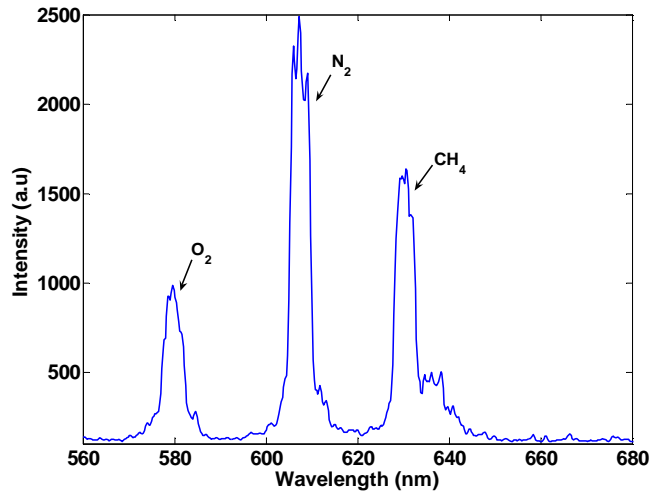


Figure 5. Typical single shot Raman spectra recorded close to injector in the SPRF combustor at  $\phi = 0.6$ .

flow rate of 8.1 g/s and an equivalence ratio of 0.58. These results were obtained by averaging 300 instantaneous PIV images. The flowfield resembles that of a confined jet, but the presence of the closed end causes the axial velocity to decay rapidly. As seen in Figure 6b, the average axial velocity ( $U$ ) drops to half its initial value by  $x=150$  mm ( $x/D=12$ ). On the other hand, the rms fluctuations ( $u'$ ) and turbulence intensity ( $u'/U$ ) rapidly increase, with the centerline intensity increasing from 0.23 to 0.5 over a small distance ( $x/D=10-12.5$ ). Thus, the unconventional geometry of the SPRF combustor ensures the existence of a region of both low ( $10^3$  m/s) average velocity and high fluctuating velocity, which should exist over a wide range of combustor loadings.

The rapid decay in velocity results from the high shear between the incoming forward flow and the reverse flow of the exiting gases. This can also lead to entrainment of exiting high temperature products and flame radicals into the incoming reactants, which can significantly enhance chemical reaction rates.<sup>8</sup> The mean chemiluminescence field shown in Figure 6c suggests that most of the heat release happens from  $x=100-200$  mm, coinciding with the low average velocity region observed in the PIV data. High  $u'$  in this midregion of the combustor creates a highly corrugated flame that can propagate against the local mean flow (which is still 20-50 m/s). Any entrainment of hot products would also act to increase the local flame speed and improve flame stability. In case of non-premixed operation of the combustor, the overall flow features are found to be similar to the premixed case (except in the near field) with the presence of a low  $U$  and high  $u'$  region in the second half of the combustor. Unlike the premixed combustor, there is negligible heat release close to the injector; the flame is completely lifted and stabilized only in the region of lower velocity and high unsteadiness as shown in Figure 6d. Any increase in hot product entrainment into the reactants due to flame liftoff would further increase reaction rates (and flame speeds), enhancing flame stabilization in the downstream regions. Additionally, the large standoff distance also suggests there is time for fuel and air to mix before reaching the flame zone hinting towards why both modes of operation have similar emission performance. Hence, the rest of the paper will be devoted to further investigate the mixing process involving fuel-air-product gas and its implications on the combustor performance.

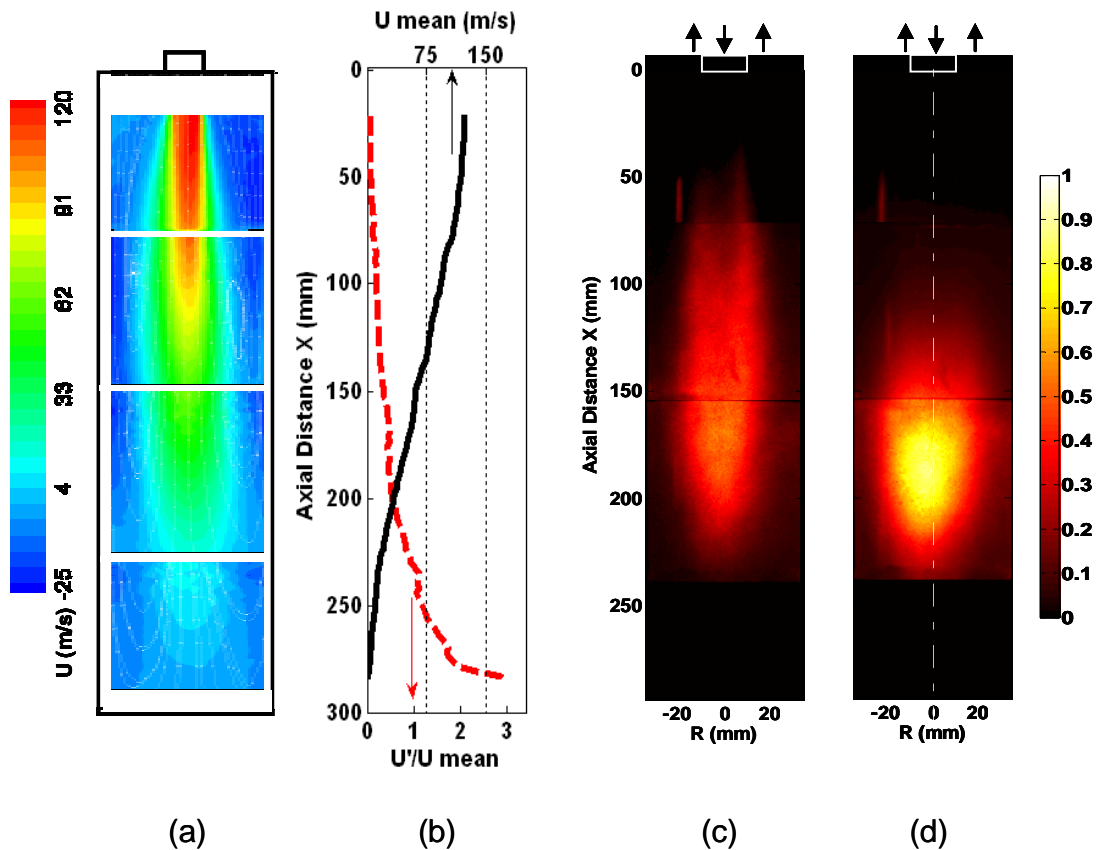


Figure 6. (a) Mean axial velocity contours, (b) mean centerline velocity and turbulence intensity profiles followed by mean chemiluminescence fields in the (c) premixed and (d) non-premixed modes of operation in the SPRF combustor at  $\phi = 0.6$  and a loading of 8.1 g/s.

## A. Product Entrainment

The possibility of hot product entrainment into the reactants before the flame front is explored with concentration measurements of the major species in the premixed SPRF combustor at the same conditions presented above (i.e., loading of 8.1 g/s and equivalence ratio of 0.6). Figure 7 shows the axial variation (averaged over 500 laser shots) of mean mole fractions of  $\text{CO}_2$  and  $\text{CH}_4$ , and the local temperature along the combustor centerline. The data extends from close to the injector to half way down the combustor length ( $x=10\text{--}160$  mm). Results show the presence of product gases ( $\text{CO}_2$ ) as early as  $x/D=4$ , even along the centerline, which suggests product entrainment starting close to the injector. It is also possible that this early appearance of product gases along the combustor centerline is due to combustion of reactant packets in the jet core. However, chemiluminescence images indicate no significant level of fuel-air burning is occurring there.<sup>14</sup> The Raman temperature measurements acquired along the centerline indicate an inlet reactant temperature of 450 K, which matches the inlet temperature measured with the thermocouple at the injector to within 30K. Beyond  $x/D=4$ , the temperature is found to increase linearly, reaching nearly the adiabatic flame temperature of 1750K in this case. Equilibrium values of the (adiabatic) flame temperature and  $\text{CO}_2$  concentration are indicated in the figure for reference.

While the average data suggest mixing of reactants and entrained products within the reactant jet, it is also possible that little mixing has occurred, and the data simply represent intermittent packets of essentially pure products. To differentiate these two interpretations, instantaneous data points acquired in pure product gases can be eliminated by conditional averaging. Pure product gases were defined to be points when the  $\text{CH}_4$  concentration is less than a threshold value chosen to be 10% of the injected global fuel fraction, which is at least twice the noise in the  $\text{CH}_4$  mole fraction measurement. The conditioned mean axial variation of  $\text{CO}_2$  and the local temperature are plotted in Figure 7. The entrainment and mixing of product gases into the reactants still starts around  $x/D=4$  and reaches significant levels before reaching the flame zone in the second half of the combustor, where most of the heat release occurs. The amount of product mixing seems to reach a plateau around  $x/D=11$ . Likewise, the distribution of the temperature of the reactants (with entrained products) in Figure 7 is quite similar to the unconditioned average close to the injector, but it saturates at  $\sim 1300$  K before reaching the heat release zone. The temperature values found after conditional averaging are lower due to elimination of data points with pure hot products.

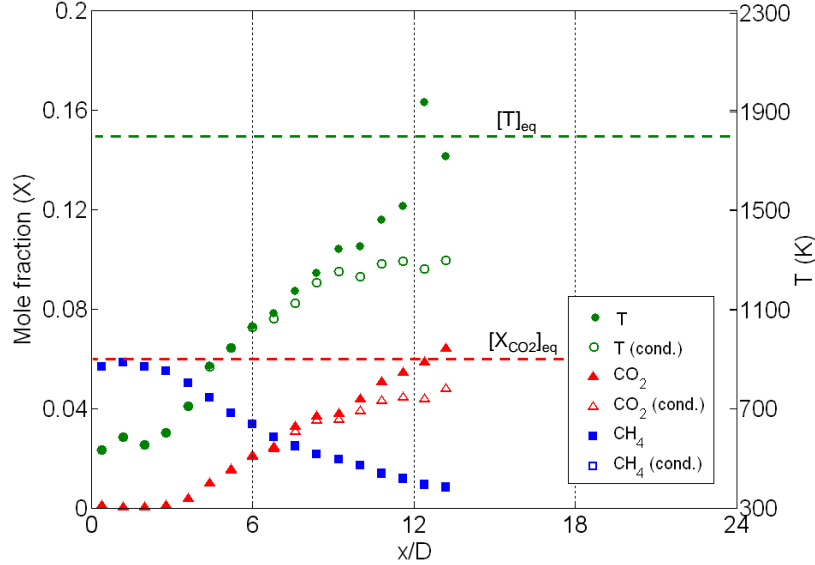


Figure 7. Axial variation of mean species mole fractions ( $\text{CO}_2$ ,  $\text{CH}_4$ ) and temperature along the combustor centerline. Conditionally averaged values of the same over data points only in the reactants are also plotted.

The recirculation ratio ( $K_v$ ) in the SPRF combustor can be calculated from the Raman measurements. For these purposes, an equivalent definition of  $K_v$  is

$$K_v = \frac{Y_{\text{CO}_2} + Y_{\text{H}_2\text{O}} + Y_{\text{O}_2,P} + Y_{\text{N}_2,P}}{Y_{\text{CH}_4} + (Y_{\text{O}_2} - Y_{\text{O}_2,P}) + (Y_{\text{N}_2} - Y_{\text{N}_2,P})}; \quad Y_{\text{O}_2,P} = \frac{w_{\text{O}_2}}{w_{\text{CO}_2}} \left[ \frac{2}{\phi} - 2 \right] Y_{\text{CO}_2}; \quad Y_{\text{N}_2,P} = \frac{w_{\text{N}_2}}{w_{\text{CO}_2}} \left[ \frac{7.52}{\phi} \right] Y_{\text{CO}_2}$$

where  $Y_i$  and  $w_i$  are the mass fraction and molecular weight of species  $i$  respectively. Further  $Y_{i,p}$  represents the mass fraction of the species  $i$  which ought to be present for a given mass of  $\text{CO}_2$ . Histograms of these fractions at six different axial locations along the combustor centerline are shown in Figure 8 for  $\phi = 0.6$ . The recirculation ratio in the SPRF combustor is found to increase (on average) with axial distance but is also characterized by a wider distribution. By  $x/D=10-12$ , packets with recirculation ratios as high as  $\sim 2$  are found. A  $K_v$  of 2 corresponds to 67% of the incoming mixture being hot products by mass. The reactant temperature at this recirculation ratio would be about 1300 K. It should also be noted that the likelihood of finding a reactant packet that has not been diluted by hot products ( $K_v = 0$ ) goes down as we move towards the flame zone suggesting good mixing between the reactants and product gases. In fact by  $x/D \sim 12$ , it is highly unusual to see any pure reactant packets.

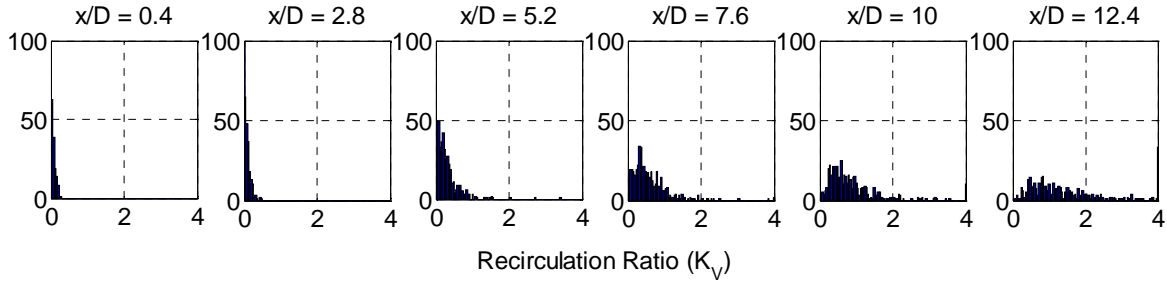


Figure 8. Histogram of recirculation ratio ( $K_v$ ) over 500 data points measured at various axial locations along the premixed SPRF combustor centerline.

The results above indicate that by the time the reactants reach the region where most of the heat release occurs, they are highly preheated and laden with radicals due to the recirculation of hot product gases. To explore the possibility that the reactants autoignite in a reactor type flow, the observed conditions have been modeled with a plug flow reactor (CHEMKIN)<sup>10</sup> and the time required for various reactant mixtures to autoignite is determined. The effect of hot product gas entrainment was simulated by adding a fraction of hot, adiabatic products (produced from a pure reactant mixture) into the inlet reactant stream. The initial reactant temperature was set to the reactant temperature determined from the injector thermocouple. The reactant temperature would further increase as hot product gases are entrained before reaching the flame zone. The ignition delay as a function of recirculation ratio in the reactant mixture is shown in Figure 9 for a range of equivalence ratios. With increasing recirculation ratio, the reactant temperature increases, reducing the ignition delays in the combustor. Also shown in the figure are three dotted lines at time delays that correspond to the average centerline flow time at a given axial location in the combustor (calculated from the mean velocity fields). The simulations suggest that time the flow has before it reaches the flame zone at  $x/D > 12$  is too short for the mixtures to autoignite at  $\phi = 0.6$ , even under the assumption that the reactants had achieved a recirculation ratio of 2 right as they entered the combustor. Thus it can be concluded that the combustion must still occur in a flame like manner.

The reactants in the SPRF combustor are highly preheated (primarily by mixing of hot products) and burning under intense turbulence. A natural question arises about the structure of the flame zone. Are the reactants burning in the thin flame front or in a distributed manner like in a reactor? The turbulent flame structure of the SPRF combustor can be analyzed with the approach developed by Borghi<sup>15</sup> and as modified by Peters.<sup>16</sup> This requires determining the total rms velocity ( $u'$ ), laminar flame speed ( $S_L$ ), integral length scale ( $L_T$ ) and flame thickness ( $\delta_L$ ).

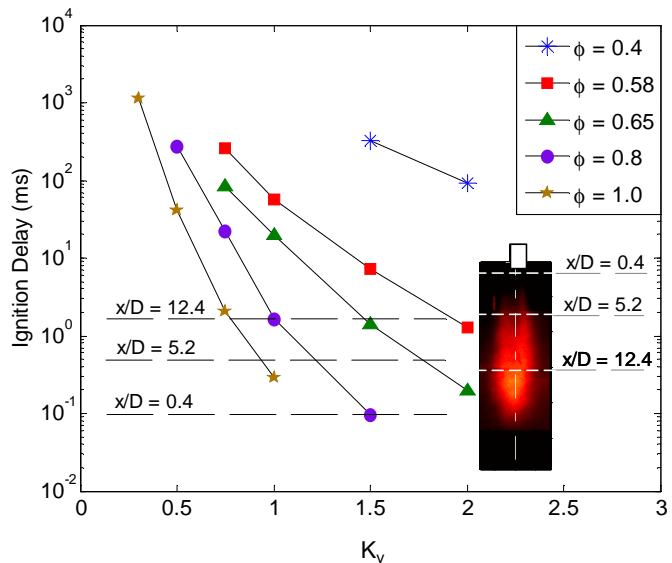


Figure 9. Variation of ignition delays in milliseconds with increasing recirculation ratios ( $K_v$ ) over a range of equivalence ratios. Flow times to reach various axial locations estimated from the mean velocity field also shown for reference.

The rms velocities were obtained from 400 instantaneous PIV images. Since only two velocity components were measured, the total rms velocity was estimated by assuming the out-of-plane velocity component was comparable to the in-plane, lateral component. Further, the integral length scale is found by integrating the turbulent velocity correlation function computed from the instantaneous velocity fields. These values are summarized in Table I.

Table I. Flow conditions and spatial locations used for regime analysis.

Equivalence Ratio, $\phi$		0.6		
Mass Loading		8.1 g/s		
Reactant Temperature, $T_{\text{react}}$		450 K		
Location	$x/D$	$r/D$	$u'_{\text{rms}}$ (m/s)	$L_T$ (mm)
1	3	1.1	14.4	2.7
2	9	1.8	13.3	5.6
3	15	0	15.9	10.4

Table II. Flame properties obtained from CHEMKIN (GRIMECH 3.0)

$K_v$	Flame Thickness $\delta_L$ (mm)	Laminar Flame Speed $S_L$ (m/s)
0	0.73	0.27
0.5	0.60	0.90
1.0	0.57	1.58
1.5	0.565	2.3
2.0	0.58	3.0

The flame speed and thickness,  $S_L$  and  $\delta_L$ , estimated with premixed, laminar flame simulations (CHEMKIN PREMIX and GRIMEch 3.0)<sup>2</sup> for various conditions are listed in Table II. The effect of hot product gas entrainment was simulated by adding a fraction (quantified by  $K_v$ ) of hot, adiabatic products (produced by a pure reactant mixture) into the inlet reactant stream. The flame structure analysis was performed for five entrainment levels ( $K_v = 0, 0.5, 1.0, 1.5$  and  $2.0$ ) and three spatial locations in the combustor. The first two locations chosen are in the shear layer, at  $x/D=3$  and 9 (or about  $1/8^{\text{th}}$  and  $3/8^{\text{th}}$  of the combustor length). These regions are highly strained due to high incoming reactant velocities and reverse flow, product gas velocities. The third spatial location is  $x/D=15$  on the centerline, where the chemiluminescence images indicate most of the heat release occurs. It can be seen from the diagram of Figure 10 that all these locations appear to fall in the thin reaction zone regime suggested by Peters.<sup>16</sup> In this region, one expects a distinct reaction zone unaffected by turbulence. For comparison, typical flames in stationary gas turbines are characterized by extremely high turbulent Reynolds numbers ( $Re_T > 10^4$ ) with  $Da \sim 1$  and  $Ka > 10$ .

The likely turbulent flame structure is seen to evolve along the combustor. Close to the injector,  $u'/S_L$  is high since there has been little chance for product entrainment, and  $L_T/\delta_L$  is low because the shear layer is thin and the vortices are smaller. As the flow moves farther from the injector,  $L_T/\delta_L$  increases and  $u'/S_L$  decreases because the characteristic eddy size increases, and because the amount of product entrainment is expected to increase (higher  $S_L$  and thinner  $\delta_L$ ). Hence we expect the combustion structure to evolve as

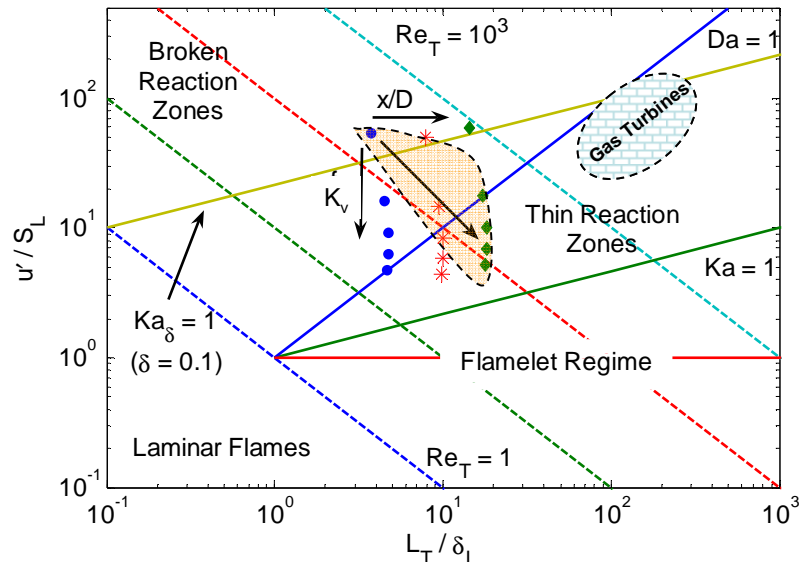


Figure 10. Estimate of turbulent combustion regimes for the SPRF combustor with points shown for conditions in Tables I and II.

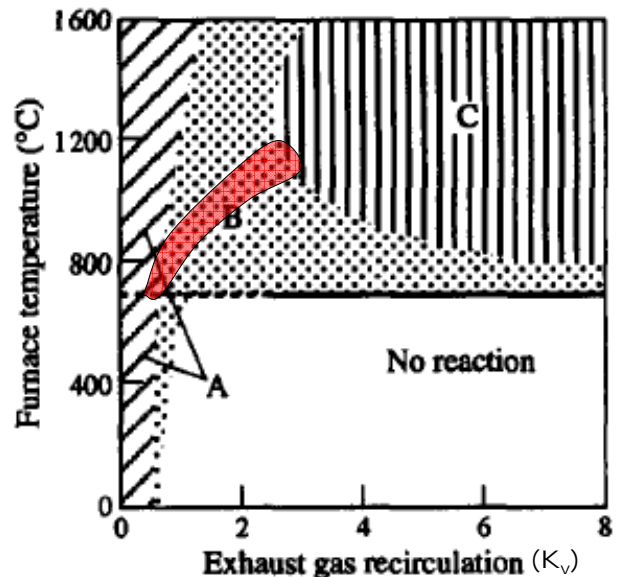


Figure 11. Schematic of flame stability limits by Wunning.<sup>1</sup> Also shown is the map of operating conditions of the SPRF combustor in red.

indicated by the diagonal arrow in Figure 10. The combustion becomes more flamelet like farther from the injector. It should be noted that the flame calculations assume recirculation/entrainment of equilibrium products. In practice, the concentrations of flame radicals in the entrained products may be higher, which would increase  $S_L$  further and push the combustion structure even closer to the flamelet regime.

To put this work in perspective with the different flame stability limits found by Wunning *et al.*,<sup>1</sup> the operating conditions of the SPRF combustor are indicated (in red) on a schematic diagram of stability limits for different combustion modes involving exhaust gas recirculation (Figure 11). In that work, the reactants entering the combustor were diluted with cooled exhaust gases and then, preheated to the furnace temperature. Thus, the extent of product recirculation and the reactant preheat temperature were controlled independently. It should be noted that in case of the SPRF combustor, the product gases are recirculated internally and not significantly preheated (reactants are at 450K) before entering the combustor. The reactant temperature rise is therefore primarily due to mixing with near adiabatic product gases inside the combustor before the flame zone. Hence, the reactant preheat temperature is strongly coupled with the recirculation ratio. Most of the heat release in the SPRF combustor occurs in the narrow band shown which falls in the unstable zone where the flame is lifted off and would blow out in other combustors. However, the recirculation of near adiabatic product gases laden with radicals along with the robust flame anchoring stagnation zone allows the SPRF combustor to operate stably at an ultra lean stoichiometry even though the flame is lifted off from the injector. The small recirculation ratio allows for a compact combustor in applications where space and weight are a concern, offering higher power densities.

## B. Fuel-Air Mixing

Due to safety concerns, a non-premixed mode of combustor operation is typically preferred. However, to maintain low emission levels, the fuel and air injected separately should have a chance to premix down to the lean global stoichiometry before the flame. Hence, the mixing of these streams is of significance to us. The shear layer between the fuel and air streams plays a vital role in the extent of premixing and thereby, affects the temperatures in the combustor and its emission levels. The effect of shear on the mixing quality is examined by making concentration measurements for two flow conditions at the same mass loading (8.1 g/s) and equivalence ratio (0.6). Case 1 corresponds to the combustor geometry used to produce the ultra low NOx reported in the previous measurements. In case 2, the air velocity is reduced by increasing the outer diameter of the air injection annulus while maintaining the same size fuel tube (and fuel velocity). The two flow conditions are summarized in Table III.

Table III. Changes in flow conditions to study the effect of air velocity on fuel-air mixing.

	Case I (High Shear)	Case II (Low Shear)
Air Tube Diameter (D, in mm)	12.5	21
Air Injection Velocity (m/s)	120	35.6
Fuel Injection Velocity (m/s)	37.2	37.2

All other conditions are held constant.

The extent of fuel-air premixing in the combustor is quantified by a single parameter, the mixture fraction ( $f$ ) as defined by Bilger.<sup>17</sup> This fraction is calculated from measured species concentrations accounting for the C and H atoms in the combustor and represents the fraction of mass in the sample that originated in the fuel jet. The mixture fraction takes values between zero and one corresponding to no fuel (pure air) and pure fuel streams respectively. The variation of mean mixture fraction ( $\bar{f}$ ) along the combustor centerline is depicted in Figure 12 for both premixed and non-premixed modes of combustor operation. In the premixed mode, the mixture fraction level is found to be constant as expected and attains the same value for both flow conditions in Table III, confirming that the combustor was operating at the same global stoichiometry. The stoichiometric and premixed injection mixture fraction levels are also shown in Figure 12 (dotted lines) for reference.

The extent of fuel-air premixing in the combustor is quantified by a single parameter, the mixture fraction ( $f$ ) as defined by Bilger.<sup>17</sup> This fraction is calculated from measured species concentrations accounting for the C and H atoms in the combustor and represents the fraction of mass in the sample that originated in the fuel jet. The mixture

fraction takes values between zero and one corresponding to no fuel (pure air) and pure fuel streams respectively. The variation of mean mixture fraction ( $\bar{f}$ ) along the combustor centerline is depicted in Figure 12 for both premixed and non-premixed modes of combustor operation. In the premixed mode, the mixture fraction level is found to be constant as expected and attains the same value for both flow conditions in Table III, confirming that the combustor was operating at the same global stoichiometry. The stoichiometric and premixed injection mixture fraction levels are also shown in Figure 12 (dotted lines) for reference.

In the non-premixed mode, where fuel and air are injected separately, the mixture fraction in Case I is found to approach the premixed value by  $x=125$  mm downstream of the injector, indicating that the injected fuel is rapidly diluted with air and products before reaching the flame zone, which starts around  $x=160$  mm (shown in blue). This can be attributed to enhanced fuel-air mixing due to high shear, allowing the non-premixed mode to operate just like the premixed case. This helps explain the low values of NOx emissions measured in the non-premixed SPRF combustor as the reactants burn at a local fuel-air ratio that is lower than the stoichiometric ratio and nearly at the global stoichiometry, leading to low flame temperatures.

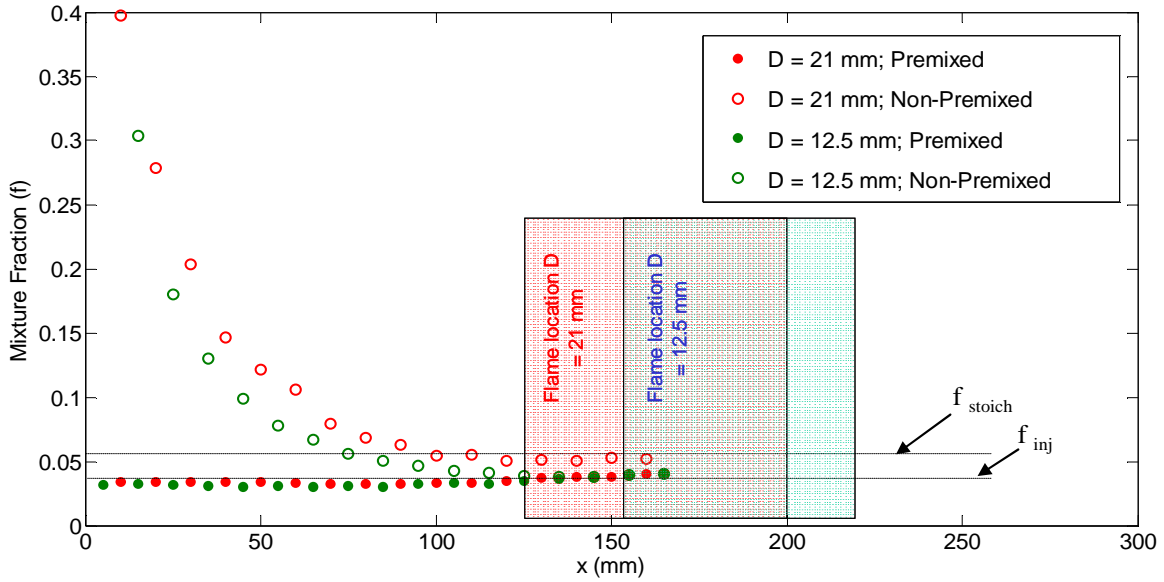


Figure 12. Axial variation of mean mixture fraction ( $f$ ) based on  $C$  and  $H$  atoms in the SPRF combustor operating at loading of  $8.1 \text{ g/s}$  and  $\phi = 0.6$  for conditions 1 and 2 shown in table III. Also shown is the location of the flame in these cases. For comparison mixture fraction values in the premixed combustor are also plotted.

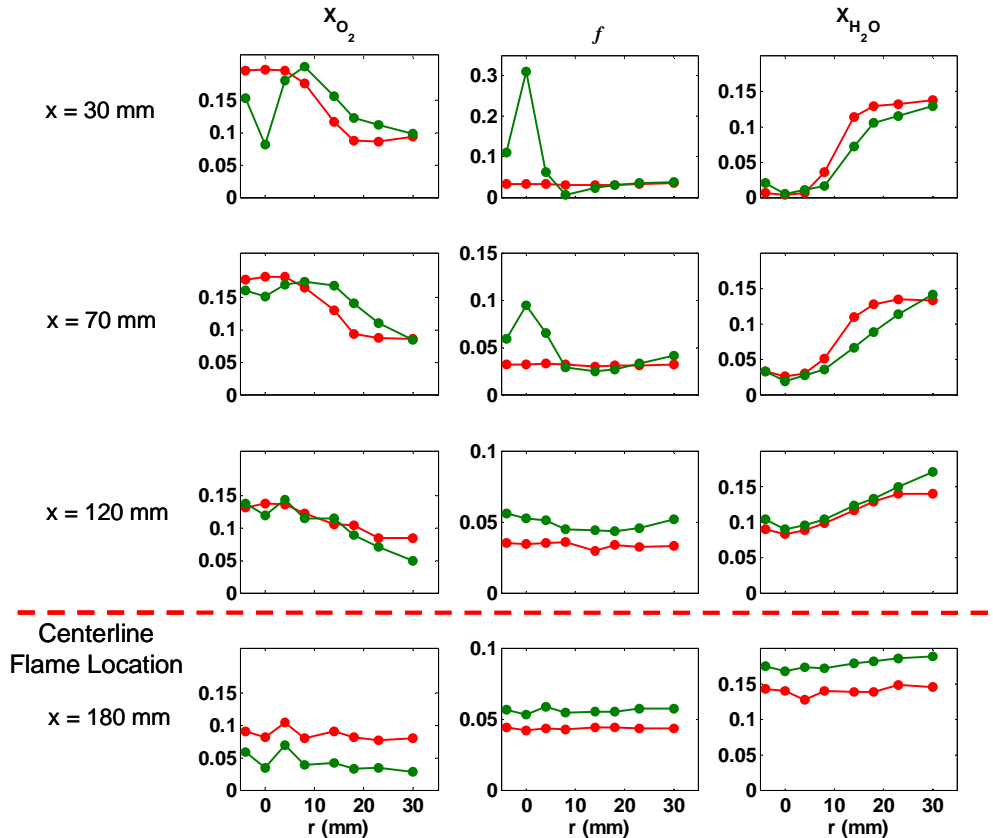


Figure 13. Radial variation of mean mole fractions of  $O_2$  and  $H_2O$  along with mixture fractions at four different axial locations in the SPRF combustor (operating at a loading of  $8.1 \text{ g/s}$ ,  $\phi = 0.6$ ) for condition 2 in table III. Variation in the non-premixed case is shown in green whereas; premixed case is shown in red. The location of the flame front along the centerline at  $x = 125 \text{ mm}$  is also marked.

In case of the 21 mm injector (Case II), where the shear is relatively low, the mean mixture fraction takes a significantly richer value relative to the premixed case. The fuel and air in this case reach the flame front (at  $x=125$  mm) in almost stoichiometric proportions along the centerline. Radial profiles of the  $O_2$ , mixture fraction ( $f$ ) and  $H_2O$  are examined in Figure 13. The profiles in the non-premixed case (shown in green) are compared to that in the premixed case (in red) at different axial distances, showing the variation across one half of the combustor. Close to the injector (at  $x=30$  mm), the fuel jet remains almost intact but the air is seen to spread out faster as seen from the higher  $O_2$  and reduced  $H_2O$  levels. At  $x=120$  mm just before reaching the flame front (at 125 mm), the fuel content indicated by the mixture fraction is not just higher along the center line, but is also higher throughout much of the combustor. This fraction seems to drop with radial distance, initially indicating that fuel and air are better mixed away from the centerline but have not completely premixed as in flow case 1. This is due to the lower shear velocity between the fuel and air. Further downstream in the flame zone ( $x = 180$  mm), all the profiles achieve a nearly constant value. A consistently higher mixture fraction in the non-premixed case indicates that some part of the air is not able to reach the flame zone but is turning around and leaving the combustor. Hence when the air velocity is reduced, this important aspect of reactant jet penetration has to be considered.

#### IV. Conclusions

The mixing and combustion characteristics of the SPRF combustor operating at atmospheric pressure have been examined in order to understand why the combustor can operate stably over a range of equivalence ratios and loadings and why low  $NO_x$  emission levels are achieved in both premixed and nonpremixed modes of operation. Various optical diagnostic techniques were employed. The results show that the combustion for both premixed and nonpremixed reactant injection is primarily stabilized in the bottom half of the combustor, where most of the heat release occurs. This region is characterized by low average velocities but intense turbulent fluctuations allowing hot product entrainment that results in stable operation of the combustor even at high loadings and very lean equivalence ratios.

Raman concentration measurements show entrainment of hot products from about 4 injector diameters into the combustor reaching an average reactant temperature of  $\sim 1300K$  just before the flame zone. This tends to increase chemical reactivity, especially of lean mixtures. Although the reaction rates are elevated due to product entrainment, the reactant mixture does not autoignite as in mild combustion due to residence times that are relatively low compared to the characteristic ignition times in the reactant/product mixture. An analysis of the turbulent combustion structure in the premixed SPRF combustor indicates that the flame is primarily in the thin reaction zone regime throughout most of the combustor. However, the flame tends to become more flamelet like farther from the injector, due to increases in the turbulent length scales and increases in the chemical rates due to entrainment of heated products and radicals into the reactants.

Fuel and air injected separately in the non-premixed mode are found to mix somewhat rapidly after entering the combustor, before significant mixing with hot products has occurred. This is facilitated by the large flame standoff seen in the non-premixed case. The effect of the air injector scaling on these mixing characteristics was also explored. Increasing the size of the outer tube of the injector decreases the shear between the fuel and air streams, which adversely affects the fuel-air mixing characteristics. It should also be noted that changing the injector size also affects reactant penetration into the combustor by affecting the velocity of the air stream. Reduced mixing and air penetration would force the fuel to burn richer than the global stoichiometry, thereby degrading the emission performance. Hence, these both these aspect need to be carefully controlled for an optimal combustor geometry.

#### Acknowledgments

This research was supported by NASA through the University Research, Engineering, and Technology Institute for Aeropropulsion and Power, under Grant/Cooperative Agreement Number NCC3-982.

#### References

- <sup>1</sup> Wüning, J. A., and Wüning, J. G., "Flameless oxidation to reduce thermal  $NO$ -formation", *Progress in Energy and Combustion Science*, Vol. 23, 1997, pp.81-94.
- <sup>2</sup> Garg A, "Specify better low  $NO_x$  burners for furnaces", *Chem. Eng. Prg*, January, pg 46-49, 1994
- <sup>3</sup> Gupta, A.K. Bolz, S. and Hasegawa, T, "Effect of Air Preheat and Oxygen Concentration on Flame Structure and Emission," *Proc. ASME J. Energy Resources and Technology*, Vol. 121, September, 1999, pp. 209-216.
- <sup>4</sup> Gupta, A. K., "Flame Characteristics with High Temperature Air Combustion," *AIAA-2000-0593*, 38th Aerospace Sciences Meeting & Exhibit, January 2000, Reno NV.
- <sup>5</sup> Kim, S-H., Yoon, Y. and Jeung, I-S., *Proc. Combust. Inst.*, 28: p463-470, 2000.

- <sup>6</sup> Smart J P, Morgan D J, "The effectiveness of multi fuel reburning in an internally staged burner of NOx reduction", *Fuel* 73, pg 1437-1442, 1994
- <sup>7</sup> Spliethoff H, Greul U, Rudiger H and Hen KRG, "Basic effects of Nox emissions in air staging and reburning at a bench scale test facility", *Fuel* 75, pg 560-564, 1996
- <sup>8</sup> J. R. Kalb and T. Sattelmayer, "Lean Blowout Limit and NOx-Production of a Premixed Sub-PPM NOx Burner with Periodic Flue Gas Recirculation," GT 2004-53410, Proceedings of ASME Turbo Expo 2004.
- <sup>9</sup> Neumeier, Y., Weksler, Y., Zinn, B. T., Seitzman, J. M., Jagoda, J. and Kenny, J., "Ultra Low Emissions Combustor with Non-Premixed Reactants Injection," AIAA 2005-3775 41st AIAA/ASME/SAE/ASEE Joint Propulsion Conference & Exhibit 10 - 13 July 2005, Tucson, Arizona.
- <sup>10</sup> Smith, G. P., Golden, D. M., Frenklach, M., Moriarty, N. W., Eiteneer, B., Goldenberg, M., Bowman, C. T., Hanson, R. K., Song, S., Gardiner Jr., W. C., Lissianski, V., and Qin, Z., GRI-Mech homepage, Gas Research Institute, Chicago, 1999, [www.me.berkeley.edu/gri\\_mech/](http://www.me.berkeley.edu/gri_mech/).
- <sup>11</sup> P. Griebel, R. Bombach, A. Inauen, R. Schären, S. Schenker, P. Siewert, "Flame Characteristics And Turbulent Flame Speeds Of Turbulent, High-Pressure," Lean Premixed Methane/Air Flames, GT2005-68565, Proceedings of GT2005 ASME Turbo Expo 2005: Power for Land, Sea, and Air June 6-9, 2005, Reno-Tahoe, Nevada, USA.
- <sup>12</sup> Nooren P A, Versluis M, van der Meer T H, Barlow R S and Frank J H, "Raman-Rayleigh-LIF measurements of temperature and species concentrations in the Delft piloted turbulent jet diffusion flame," *Appl. Phys. B* 71, 2000, 95-111
- <sup>13</sup> Miles P C, "Raman line-imaging for spatially and temporally resolved mole fraction measurements in internal combustion engines", *Appl. Opt.* 38 (1999)1714-32
- <sup>14</sup> Mohan K. Bobba, P. Gopalakrishnan, J. M. Seitzman and B. T. Zinn, "Characteristics of Combustion Processes in a Stagnation Point Reverse Flow Combustor," GT2006-91217 in Proceedings of the ASME/IGTI Turbo Expo 2006, Barcelona, Spain May 8-11, 2006
- <sup>15</sup> Borghi R., *Recent Advances in Aerospace Science*, ed C Bruno and S Casci, 1985, p. 117.
- <sup>16</sup> Peters, N., *J. Fluid Mech* 384 (1999) 107-132.
- <sup>17</sup> Bilger, R. W., *Twenty-Second Symposium (International) on Combustion*, The Combustion Institute, Pittsburgh, 1988.